IEEE Access
Multidisciplinary | Rapid Review | Open Access Journal

Received January 19, 2020, accepted February 12, 2020, date of publication February 17, 2020, date of current version February 27, 2020.

Digital Object Identifier 10.1109/ACCESS.2020.2974407

Implementation of Vector Hysteresis Model Utilizing Enhanced Neural Network Based on Collaborative Algorithm

LIANQIANG CHI[1], DIANHAI ZHANG[1], MENGFAN JIA[2], AND ZIYAN REN[1]
[1]School of Electrical Engineering, Shenyang University of Technology, Shenyang 110870, China
[2]Hunan Provincial Engineering Research Center for Electric Vehicle Motors, CRRC Zhuzhou Electric Company, Ltd., Zhuzhou 412000, China

Corresponding author: Dianhai Zhang (zdh700@126.com)

This work was supported in part by the National Natural Science Foundation of China under Grant 51707125, and in part by the Program funded by the Ministry of Education in Liaoning Province under Grant LR2017060.

ABSTRACT A hysteresis model, based on the enhanced neural network with parallel strategy, is put forward for the prediction of the accurate magnetic behavior of electrical steel sheets (ESSs). Aimed at overcoming the drawbacks such as low convergence rate and convenient to trap into local optimum in the conventional back-propagation neural network (BPNN), a novel collaborative BPNN learning algorithm is introduced according to the error back propagation mechanism and particle swarm optimization (PSO). The reasonable selection of the test point set by the uniform design of experiment methodology, has the potential of lowering the measurement cost, together with guaranteeing the accuracy of the hysteresis modeling. A parallel strategy, which is based on the fast Fourier transformation (FFT), is applied for enhancing the train efficiency of BPNNs. The proposed algorithm is applied for the purpose of modeling the vector hysteresis behavior of ESS. Together, the comparison of the measured and predicted results of H-locus and core loss is discussed as well.

INDEX TERMS Back-propagation neural network, collaborative algorithm, design of experiment, parallel strategy, particle swarm optimization, vector hysteresis model.

I. INTRODUCTION

The electric machines that have high power density and efficiency are being required in not just an electric traction system but the general industrial area as well. In order to cater to these requirements, in the design phase of electric machines, an accurate magnetic field analysis is deemed as essential, which considers the rotating magnetic field as well as the alternating one. As it is fully known the rotating magnetic fields leave a significantly more impact on the core loss in comparison with the alternating one [1]. The behavior of the rotating magnetic fields could be analyzed with the help of a coupling vector hysteresis model with performance analysis according to the finite element method (FEM).

The majority of the previous research works, for instance, the generalized Jiles-Atherton model, Preisach model [2]–[6] and Play model [7]–[9], puts efforts into making use of less measurement data for their simplicity. Nonetheless, it is, significantly hard expecting the high accuracy with the less experimental data. Conversely, the E&S model is put forward according to the extensive amount of experimental data. Nevertheless, its reluctivity expression is significantly hard extending to the higher harmonic components for the enhancement of accuracy [10]–[12]. Some research works have introduced neural networks (NN) in hysteresis modeling, meanwhile, being constrained to the alternating magnetic field condition [13]–[20]. The NN and actual frequency transplantation are combined for the purpose of predicting the hysteresis when the exciting field is highly contaminated by harmonics [13]. The current paper puts forward a methodology based on genetic algorithms and NN, which is suitable for finding the five parameters of the Jiles–Atherton model for generalization to the dynamic hysteresis loops [14]. A method of hysteresis loop evaluation based on NN and Fourier Descriptor technique is put forward. The dependence of the hysteresis loop from the magnetic field frequency, is evaluated by NN, on the other hand, with the help of the Fourier Descriptor, the effects of the magnetic field distortion

The associate editor coordinating the review of this manuscript and approving it for publication was Jiahu Qin.

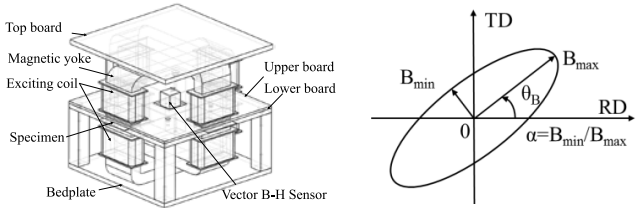

(a) Measurement apparatus (b) Parameter definition

FIGURE 1. Measurement apparatus and parameter definition.

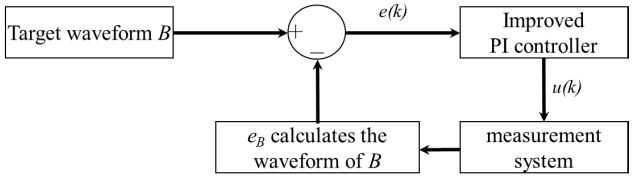

FIGURE 2. Block diagram of *B* waveform digital feedback control system.

are predicted [15]. An NN to implement a hysteresis model for a magnetic material within a finite element program is described as well [16]. A methodology, based on NN and a multidimensional optimization procedure, is put forward for lowering the time taken and for enhancing the accuracy in the evaluation of the parameters of the Jiles–Atherton model of magnetic hysteresis [17]. A dynamic hysteresis model, based on NN, is put forward, which is capable of carrying out the simulation of any kind of dynamic loop generated by any of the assigned arbitrarily distorted excitations into a fixed range of frequencies [18]. A scalar hysteresis model, based on NN, put forward for the purpose of modeling the behavior of magnetic materials [19]. An Ising hysteresis model is put forward on the basis of NN aimed at predicting the effect of the temperature, the field amplitude and the field frequency on the hysteresis properties [20]. Recently, some scholars have developed the vector magnetic hysteresis model in accordance with the conventional NN [21], [22], nonetheless, in the papers, the conventional feed-forward NN (FFNN) is applied, and the inherent shortcomings of the FFNN are not taken into account, for instance, easier to fall into the local minima.

The current paper puts forward an enhanced back-propagation neural network (BPNN) model with parallel strategy for the modeling of the vector hysteresis properties of electrical steel sheets (ESSs). The proposed model has parallel networks for each of the harmonic components for not just lowering the training efforts but augmenting the prediction accuracy as well. In the learning mechanism, the model adopts the error back propagation mechanism, combined with the particle swarm optimization (PSO) algorithm. The training data are attained from the B- and H-waveforms that are experimentally measured with the help of a self-developed two-dimensional single sheet tester.

II. VECTOR MAGNETIC PROPERTIES MEASUREMENT

A. MEASUREMENT APPARATUS

Fig. 1(a) sheds light on the measurement apparatus of vector magnetic properties for ESS. Both the rotating magnetic field and alternating magnetic field could be generated and measured by using this apparatus. The elliptic rotating magnetic flux density locus is defined in accordance with the three characteristic parameters, that include the maximum magnetic flux density B_{max}, magnetization angle θ_B, and the axis ratio α, as illustrated in Fig. 1(b). B_{max} represents the maximum value of the flux density vector in the elliptic locus. α is the ratio of B_{min} to B_{max}. θ_B is defined as the inclined angle between B_{max} and RD direction. With regard to each of the measurement cases, the magnitude and the initial phase (fundamental and higher harmonic components) of H-waveform are stored by the fast Fourier transformation (FFT).

Owing to the nonlinearity of the magnetic properties of ESS, the B waveform is distorted subjected to the strong sinusoidal excitation. In the relevant magnetic characteristic measurement standard, the measured B typically requires a sinusoidal waveform. That is why, in the current paper, B-waveform is controlled to be sinusoidal. A feedback control system is developed between the excitation voltage waveform $u(k)$ and B, together with applying the Proportional-Integral (PI) control algorithm. Eventually, through the adjustment of the excitation voltage waveform signal $u(k)$ and induced voltage of B-probe e_B, a sinusoidal B waveform, satisfying the measurement criterion is attained. The schematic diagram of its feedback control system is illustrated in Fig 2.

The detection of the magnetic flux density signal is fulfilled based on a probe method. In the current paper, four retractable metal probes are employed for the purpose of detecting the flux density signals along rolling direction (RD) and transverse direction (TD). The magnetic field strength signals are picked up with the use of the H-coil methodology. The double composite H-coils are applied for detecting the magnetic field strength signals along RD and TD, simultaneously. The surface magnetic field intensity signal of the sample cannot be directly measured by just one composite H-coil for the small gap between sample and coil frame. Accordingly, the double composite H-coil method mandatorily required to be adopted. The double composite H-coil method refers to the detection of the magnetic field strength signal at different positions above the measurement sample by the two sets of composite H-coils; accordingly, the magnetic field strength of the sample surface could be calculated according to the extrapolation algorithm. Fig. 3 demonstrates the physical device of the vector B-H sensor and the diagrammatic sketch of the B-probe and H-coil.

B. DESIGN OF EXPERIMENT

The quality of hysteresis modeling depends on not just the testing data but their accuracy as well. In general, the measurement conditions are selected by uniform sampling with

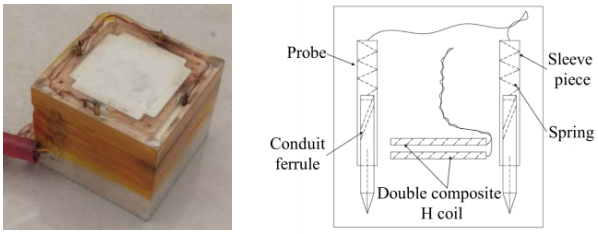

(a) physical device (b) diagrammatic sketch

FIGURE 3. Vector B-H sensor.

TABLE 1. Measurement conditions.

Variable	Different Cases									
B_{max} (T)	0.5	0.5	0.5	0.6	0.6	0.6	0.7	0.7	0.7	0.8
θ_B (°)	60°	20°	80°	40°	0°	60°	20°	90°	50°	10°
α	0.8	0.4	0	1	0.6	0.2	1	0.8	0.4	0
B_{max} (T)	0.8	0.8	0.9	0.9	0.9	1.0	1.0	1.0	1.1	1.1
θ_B (°)	70°	30°	90°	50°	10°	80°	40°	0°	60°	20°
α	0.8	0.6	0.2	1	0.6	0.4	0	0.8	0.4	0.2
B_{max} (T)	1.1	1.2	1.2	1.2	1.3	1.3	1.3	1.4	1.4	1.4
θ_B (°)	80°	40°	0°	70°	30°	90°	50°	10°	70°	30°
α	1	0.6	0.2	0	0.8	0.4	0	1	0.6	0.2

the same interval among all of the factors. For instance, according to the typical operating conditions of ESSs, the measurement condition in the current paper is set as hereunder: B_{max} varies from 0.5T to 1.4T with the interval of 0.1T; α changes from 0 to 1 with the interval of 0.2, and θ_B is from 0° to 90° with the interval of 10°, correspondingly. If the whole factor design of experiment (DOE) methodology is employed, in aggregate, there are 600 measurement conditions. Typically, it takes approximately 0.5 hours for measuring a case, besides taking almost 12 days for measuring all of the 600 cases. There is significantly huge measurement burden. Accordingly, the whole factor DOE methodology is not applicable.

Together with the whole factor design of experiment method, the DOE schemes include the orthogonal design of experiment and uniform DOE method. The orthogonal DOE is suitable for the experiments that have a few levels (a few measurement conditions in each factor). For the high number of levels, in the current work, the orthogonal DOE cannot be applied.

Adopting the uniform DOE method, just 30 measurement conditions are required by referring to the uniform design table. The measurements, which are selected by this scheme, are illustrated in TABLE 1. The uniform DOE method is put forward by K. Fang and Y. Wang [23], [24]. In comparison with the orthogonal design, the uniform design is deemed as more suitable for the complex experiments having a large span of test range, in addition to a number of factors. The existence of uniform design table makes it quite convenient applying the uniform design.

C. MEASUREMENT RESULTS

Through the aforementioned measurement apparatus, the magnetic characteristics of non-oriented ESS B50A600 are measured under the frequency of 50Hz based on TABLE 1. As Fig. 4 demonstrates, even for the non-oriented ESS, the magnetic properties are anisotropic.

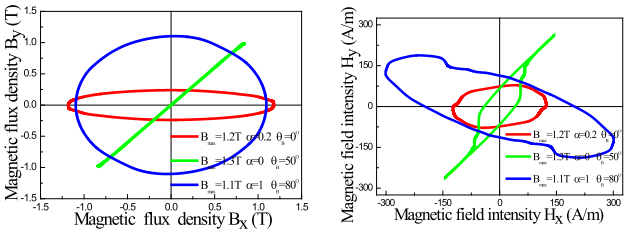

(a) Locus of the B vector (b) Locus of H vector

FIGURE 4. Measurement results.

III. VECTOR HYSTERESIS MODELING

A. NEURAL NETWORK

An artificial neural network is a massively parallel distributed processor, comprising one or more neurons. Neurons refer to the basic information processing units for the neural network operations, besides constituting the basis for designing neural networks. The input of the neuron is multiplied by the corresponding weight, weighting and summing, and subsequent to that, the output of the neuron is generated by the transfer function. Transfer functions include the linear transfer functions and nonlinear transfer functions. The neurons are arranged linearly in a so-called layer and then connected to other layers. Through the selection of the number of layers, the number of neurons per layer, and the type of transfer function, the optimal neural network for a specific problem could be created.

The Back Propagation (BP) network refers to a multilayer feed forward network, which is a kind of error back propagation network, and it is counted among the most extensively employed neural network models. The BP network comprises an input layer, some hidden layers and an output layer. Without the limitation of the number of hidden layer nodes, a BP network with just one hidden layer is capable of implementing any nonlinear mapping. The neurons are connected between the layers and layers by a full interconnection, and the neurons between the same layer are not connected to each other.

The learning of BP network comprises two stages: the first stage involves the input of the known learning samples through the hidden layer, followed by calculating the actual output value of each neuron. This stage is termed as the forward propagation process and the other stage is called the back-propagation process. It refers to the process of the adjustment of the weight and threshold value. The difference (error) between the actual output and the expected output is calculated, together with propagating the error back to the layer by layer, which modifies the weight threshold of the network according to the gradient descent methodology. The two processes are repeated alternately, eventually minimizing the error function. The updated formula for weights and

threshold values is presented as hereunder:

$$v_{kj}(t+1) = v_{kj}(t) + \lambda\delta_k H_j \tag{1}$$
$$w_{jh}(t+1) = w_{jh}(t) + \lambda\sigma_j I_h \tag{2}$$
$$B_k(t+1) = B_k(t) + \beta\delta_{\mathrm{k}} \tag{3}$$
$$b_{\mathrm{j}}(t+1) = b_{\mathrm{j}}(t) + \beta\sigma_{\mathrm{j}} \tag{4}$$

where $v_{kj}(k = 1, 2, \ldots, N_{\mathrm{o}}; j = 1, 2, \ldots, N_{\mathrm{h}})$ indicates the weight between the hidden node j and the output layer node k, $w_{jh}(j = 1, 2, \ldots, N_h; h = 1, 2, \ldots, N_i)$ refers to the weight between the input node h and the hidden layer node j; B_k denotes the threshold of the output layer node k, and, b_j stands for the threshold of the hidden layer node j. H_j denotes the output of the hidden node j; I_h represents the input of input node h; λ and β are learning rates, correspondingly; t denotes the number of iterations; δ_k is the error of the output node k; and σ_j indicates the error of the hidden node j.

The above standard BP network is optimized in accordance with the gradient descent method, usually having a slow convergence rate, together with being convenient to fall into local optimum. For the purpose of searching the global optimum, a number of improvement strategies regarding the traditional global optimizer have been put forward, for instance, particle swarm optimization (PSO), genetic algorithm, and differential evolution. For example, the PSO methodology is employed for the replacement of the gradient descent methodology of BP network, aimed at optimizing the network connection weight as well as threshold values. The position and velocity vector are updated as hereunder:

$$X_i(t+1) = X_i(t) + V_i(t+1) \tag{5}$$
$$V_i(t+1) = \eta(t)V_i(t) + c_1 r_1 \left[P_i(t) - X_i(t)\right] + c_2 r_2 \left[P_g(t) - X_i(t)\right] \tag{6}$$
$$\eta(t) = \eta_{\max} - t \cdot (\eta_{\max} - \eta_{\min})/t_{\max} \tag{7}$$

where c_1 and c_2 refer to the learning factor; η indicates the inertia weight; r_1 and r_2 represent the two random numbers; P_i and P_g are the individual extremum and global extremum, correspondingly.

Most of the network weight adjustments of this algorithm are directly optimized by the PSO iterative algorithm, nonetheless, as the results indicate, the particles in particle swarm often gather, resulting into the premature phenomenon. Accordingly, the direct use of PSO algorithm for BP network optimization is also expected to cause the network to easy to fall into local extremum. This paper not just combines the PSO with the BP algorithm but also puts forward a collaborative network learning algorithm.

B. VECTOR HYSTERESIS MODEL BASED ON COLLABORATIVE ALGORITHM

The conventional BPNN is extensively applied in the different kinds of engineering fields. Nonetheless, in practical applications, the algorithm typically has some inherent flaws such as lower convergence rate as well as easier to fall into local minima. For the avoidance of these drawbacks, a collaborative network learning algorithm, based on PSO and back-propagation, is put forward. PSO refers to a type of global optimization algorithm, and its multi-point search pattern is capable of enhancing the global search capability and convergence speed. Accordingly, introducing the PSO algorithm to search weight and threshold coefficients could overcome the flaws associated with the conventional BP algorithm. In the meantime, the mechanism of error backward propagation is introduced into PSO algorithm, which could further enhance the search capability.

TABLE 2. Test conditions.

case	B_{max} (T)	θ_B (°)	α	case	B_{max} (T)	θ_B (°)	α
1	1.2	30°	0	7	1.3	45°	0.2
2	1.2	30°	0.6	8	1.3	45°	0.4
3	1.2	30°	1	9	1.3	45°	0.6
4	0.8	0°	0	10	1	90	0.2
5	0.8	0°	0.4	11	1	90	0.6
6	0.8	0°	0.6	12	1	90	1

When the cooperative algorithm employed for training the neural network, the parameters of the network are regarded as the position vector of the particles in the particle swarm. N_i, N_h, and N_o refer to the numbers of the neurons in input, hidden, and output layers, correspondingly; subsequent to that, the network determined by the position vector of the i_{th} particle could be demonstrated as hereunder:

$$X_i = \left(v_{11}, v_{12}, \ldots, v_{N_O N_h}, w_{11}, w_{12}, \ldots, w_{N_h N_i}, B_1, \ldots, B_{N_O}, b_1, \ldots, b_{N_h}\right) \tag{8}$$

In the proposed algorithm, the back propagation is introduced in the PSO algorithm. In accordance with the weight value and the threshold value of per layer of the neural network, the location updating formula of PSO is enhanced and (9) utilized for updating the position of the particles in order to realize the optimal adjustment and updating of the network parameters. In the process of optimization, the global search performance of the PSO algorithm is entirely utilized, and the back-propagation characteristic of the BP algorithm itself is effectively maintained as well. The position of i_{th} particle is updated as hereunder:

$$X_{im}(t+1) = \begin{cases} X_{im}(t) + V_{im}(t+1) + \lambda\delta_k H_{j1} \\ \quad if\ m \in (0, L_1] \\ X_{im}(t) + V_{im}(t+1) + \lambda\sigma_{j2} I_h \\ \quad if\ m \in (L_1, L_2] \\ X_{im}(t) + V_{im}(t+1) + \beta\delta_{k1} \\ \quad if\ m \in (L_2, L_3] \\ X_{im}(t) + V_{im}(t+1) + \beta\sigma_{j3} \\ \quad if\ m \in (L_3, L_4] \end{cases} \tag{9}$$

$$V_{im}(t+1) = \eta(t)V_{im}(t) + c_1 r_1 \left[P_{im}(t) - X_{im}(t)\right] + c_2 r_2 \left[P_{gm}(t) - X_{im}(t)\right] \tag{10}$$

$$D = N_o N_h + N_i N_h + N_h + N_o \tag{11}$$

where $m = 1,2, \ldots, \mathrm{D}$; $L_1 = N_\mathrm{o}N_\mathrm{h}$; $L_2 = L_1 + N_\mathrm{i}N_\mathrm{h}$; $L_3 = L_2 + N_\mathrm{o}$; $L_4 = L_3 + N_\mathrm{h}$; $k = \lceil m/N_\mathrm{h} \rceil$; $j_1 = m - (k-1)N_\mathrm{h}$; $j_2 = \lceil (m - L_1)/N_\mathrm{i} \rceil$; $h = m - L_1 - (j_2 - 1)N_\mathrm{i}$; $k_1 = m - L_2$; and $j_3 = m - L_3$.

$$\delta_k = (T_k - O_k)\, O_k\, (1 - O_k) \tag{12}$$

$$\sigma_j = \sum_k \delta_k w_{kj} H_j \left(1 - H_j\right) \tag{13}$$

where the T_k denotes the target output of the sample at the output node k, O_k and H_j stand for the actual output values of the output node k and the hidden node j of the sample in the network, correspondingly. The formula for the calculation of the output of hidden layer is demonstrated as hereunder:

$$H_j = F\left[\sum_{h=1}^{N_i} w_{jh} I_h + \mathrm{b_j}\right] \tag{14}$$

where F suggests activation function. The output calculation formula of the output layer is presented as hereunder:

$$O_k = \sum_{j=1}^{N_h} v_{kj} H_j + B_k \tag{15}$$

With regard to an optimization problem to be minimized, the individual extremum of each particle is updated on the basis of the formula presented as follows:

$$p_{im}(t+1) = \begin{cases} x_{im}(t+1), & f(x_{im}(t+1)) \le f(p_{im}(t)) \\ p_{im}(t), & f(x_{im}(t+1)) > f(p_{im}(t)) \end{cases} \tag{16}$$

where $f()$ denotes the fitness function defined as hereunder:

$$f_j = \frac{1}{2N} \cdot \sum\nolimits_{j=1}^{N} e_j^2(x) \tag{17}$$

where $e_j(\mathbf{x})$ denotes the error of j_th neuron and N represents the number of samples. In addition, the global extremum of all particles is updated as hereunder:

$$p_{gm}(t+1) = \arg\min\nolimits_{p_{im}(t+1)} \{f\,[p_{im}(t+1)]\} \tag{18}$$

The numerical implementation of cooperative algorithm in the current is demonstrated in Fig.5. As a matter of fact, the proposed collaborative algorithm is quite flexible. Together with the PSO, it could be combined with any other global optimizer like genetic algorithm and differential evolution. Concerning the space limit, in the following contents, only the results attained by PSO and BP are provided and discussed.

For the verification of the availability of the algorithm, three standard test functions named by Ackley function in (19), Griewank function in (20), and Rastrigin function in (21) are selected. The Ackley function has many local optima with a global optimum at 0. The Griewank function is a complex oscillation function with multiple peaks. The Rastrigin function is composed of De Jong's function and cosine function, which owns stronger nonlinearity and many local

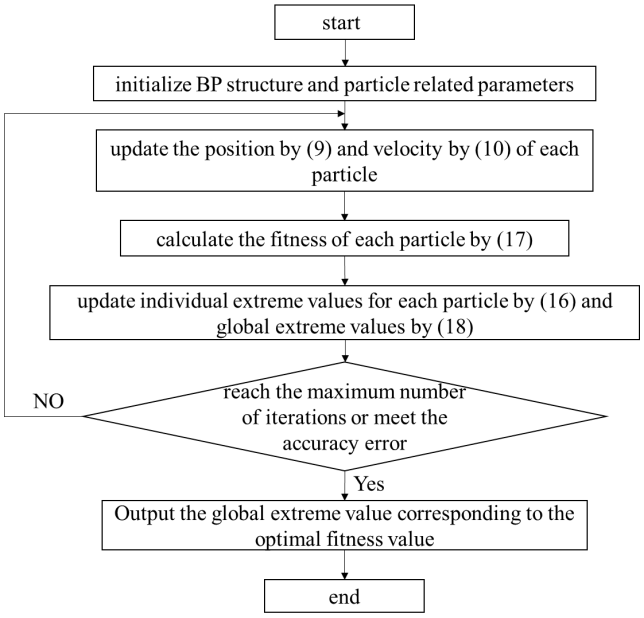

FIGURE 5. The implementation step of the collaborative algorithm.

optima. They are optimized based on the collaborative algorithm as well as the conventional BP algorithm and conventional PSO-BP algorithm, and the algorithm performance is compared as illustrated in Fig. 6.

$$f(\mathbf{x}) = -20\exp\left[-0.2\sqrt{\frac{1}{n}\sum_{i=1}^{2} x_i^2}\right] - \exp\left[\frac{1}{n}\sum_{i=1}^{2}\cos(2\pi x_i)\right] + 20 + \exp(1)\; x \in [-32, 32] \tag{19}$$

$$f(\mathbf{x}) = \frac{1}{4000}\sum_{i=1}^{n} x_i^2 - \prod_{i=1}^{n}\cos\left(\frac{x_i}{\sqrt{i}}\right) + 1 x \in [-600, 600] \tag{20}$$

$$f(\mathbf{x}) = 10n + \sum_{i=1}^{n}\left[x_i^2 - 10\cos(2\pi x_i)\right] x \in [-5.12, 5.12] \tag{21}$$

As evident from Fig. 6, as compared with the conventional BP learning algorithm and conventional PSO-BP algorithm, the collaborative algorithm put forward in the current paper, could attain the higher network learning accuracy, in addition to overcoming the flaws associated with the convergence accuracy of the traditional methodology.

C. TRAINING PROCESS WITH PARALLEL STRATEGY

As mentioned earlier, the H-waveform is distorted under sinusoidal B-waveform due to saturation. In other words, there are abundant higher harmonics in H-waveform. In general, in hysteresis model, the B-waveform is taken as input and H-waveform is taken as the output of the model. The sinusoidal B vector can be described by B_max, α, and θ_B. The non-sinusoidal H-waveform can be expressed as the sum of fundamental component and higher harmonic ones,

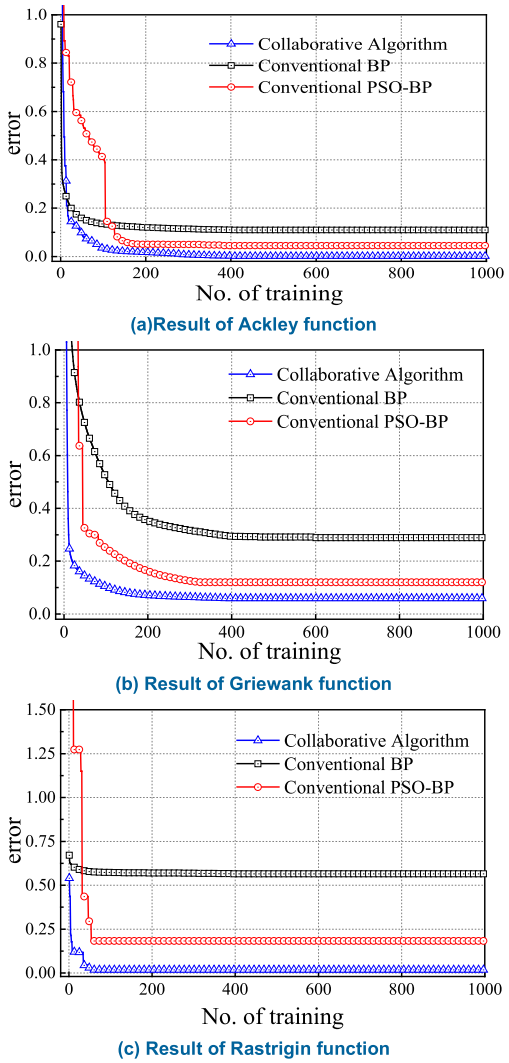

FIGURE 6. Performance comparison of different algorithms.

as hereunder:

$$\begin{cases} H_x(t) = \sum_{i=1}^{N} H_{xi} \cos(i\omega t + \varphi_{xi}), \\ H_y(t) = \sum_{i=1}^{N} H_{yi} \cos(i\omega t + \varphi_{yi}), \quad (i = 1, 3, \ldots, N) \end{cases} \tag{22}$$

According to our experience, it is essential that the higher harmonic components are remain until to 15^{th} to express the real H-waveform accurately. Furthermore, in the light of the characteristic of H-waveform, only odd harmonic components should be considered in the model. For these reasons, the number of input node N_i is 3 and the one of output node N_o is 32, as presented in Fig. 7. Based on the empirical formula, the number of hidden layer node N_h is determined to be 14, the total number of the weight and threshold value, requiring optimization is $3^*14+14+14^*32+32 = 536$, that would take significant amount of time for the solution of this kind of a high dimension problem through the optimization algorithm proposed in this paper.

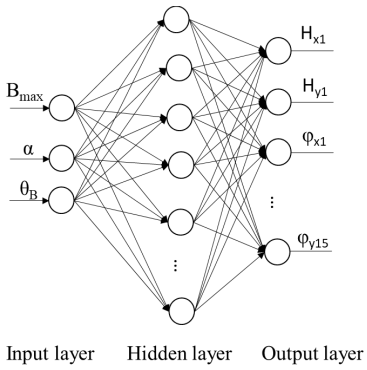

FIGURE 7. Original network structure.

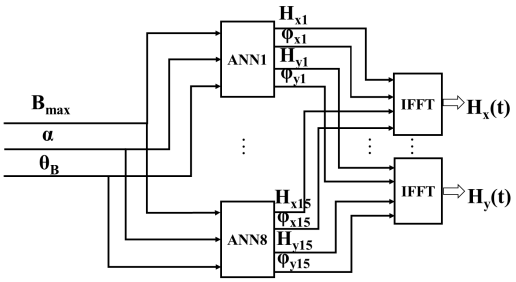

FIGURE 8. The proposed parallel training process.

Aimed at lowering the cost of training time, the present paper splits output parameters into 8 categories on the basis of harmonic orders, as illustrated in Fig. 8. B_{max}, α, and θ_B refer to the input of the neural network. The amplitude and phase of the fundamental wave of vector H-waveform are taken as the output of the ANN1, and the ones of the third harmonic of vector H-waveform are taken as the output of the ANN3, and so on. Eventually, the frequency domain prediction results of the H_x and the H_y are transferred into $H_x(t)$ and $H_y(t)$ by inverse FFT.

The eight sub-networks are independent of each other, besides sharing the same training sample set. The structure of each network is 3-7-4. The weight and threshold value requiring optimization for each network is $3^*7+7+7^*4+4 = 60$, and the reduction of dimension lowers the difficulty of network training, whereas 8 independent networks could be trained in the parallel way on the server, thereby considerably lowering the cost of training time. The transfer function of hidden layer neuron is tansig(), whereas the transfer function of output layer neuron is purelin(). They could be trained at the same time. Accordingly, both the difficulty and calculating cost of network training could be lowered considerably. Together, establishing the model replaces the large-scale measurement data, besides having the ability to better predict the unknown data.

IV. RESULTS AND DISCUSSION

In this section, the certain example is put to use for the purpose of further verifying the accuracy of the model. With the use of a single hidden layer network structure, N_i is 3, N_h is 7, N_o is 4, and the training set is 30 sets of data, with the remaining data of model for the purpose of testing

TABLE 3. Comparison of the iron loss values with different algorithms.

case		1	2	3	4	5	6	7	8	9	10	11	12
iron loss (W/kg)	Measurement	3.291	4.645	6.908	1.607	2.313	2.644	4.138	4.604	5.426	2.845	3.600	4.818
	Collaborative Algorithm	3.281	4.624	7.093	1.570	2.301	2.608	4.101	4.571	5.410	2.822	3.580	4.806
	Conventional BP	2.943	4.213	7.201	1.543	2.521	2.447	4.315	4.326	5.145	3.095	3.307	5.165
	Conventional PSO-BP	3.146	4.787	6.757	1.564	2.387	2.585	4.043	4.742	5.537	2.703	3.758	4.695
error (%)	Collaborative Algorithm	0.304	0.452	2.678	2.302	0.519	1.362	0.894	0.717	0.295	0.808	0.555	0.249
	Conventional BP	10.574	9.300	4.241	3.983	8.993	7.451	4.277	6.038	5.179	8.787	8.139	7.202
	Conventional PSO-BP	4.406	3.057	2.186	2.676	3.199	2.231	2.296	2.997	2.046	4.991	4.389	2.553

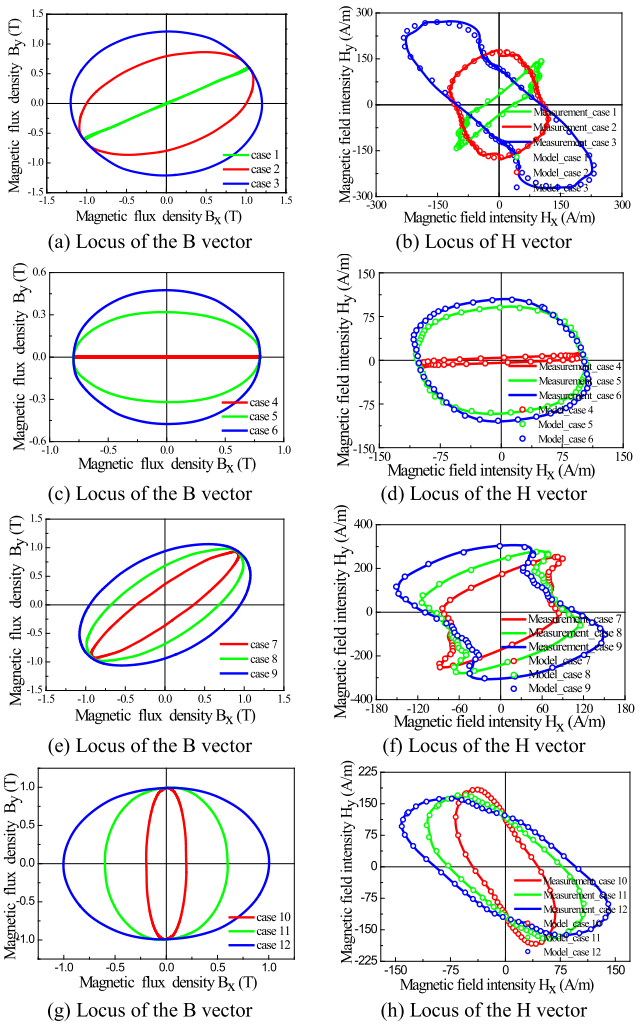

(a) Locus of the B vector (b) Locus of H vector
(c) Locus of the B vector (d) Locus of the H vector
(e) Locus of the B vector (f) Locus of the H vector
(g) Locus of the B vector (h) Locus of the H vector

FIGURE 9. The comparison measurement and model results.

the accuracy of neural network model. The comparison of measured and calculated results is illustrated in Fig. 9, and the test condition is highlighted in the TABLE 2.

The calculation formula for the iron loss of ESS is demonstrated in (23).

$$P_c = \frac{1}{\rho T}\int_T \left(h_x(t)\frac{db_x(t)}{dt} + h_y(t)\frac{db_y(t)}{dt}\right)dt \quad (W/kg) \tag{23}$$

where ρ refers to the mass density of ESSs.

The iron loss of test conditions is calculated by the proposed collaborative algorithm, traditional PSO-BPNN and conventional BPNN model, respectively. The calculation and measured results are compared and the errors are demonstrated in TABLE 3. From the comparison results, the proposed algorithm shows the best prediction under the most test conditions.

As Fig. 9 highlights, in the region where the magnetic field intensity waveform is not smooth, the error existing between the model curve and the measurement curve is large, mainly for the reason that the weights and threshold of ANN7 and ANN8 have not discovered the optimal solution; conversely, the amplitude and phase of the high order harmonics of ANN7 and ANN8 correspond to the magnetic field intensity waveform. In some of the cases, the error between the calculated value and the measured value of iron loss in TABLE 3 is comparatively larger. In addition, the reason giving rise to two problems highlighted earlier is that the training algorithm of neural network is insufficiently perfect, whereas the optimization algorithm of the network also requires additional enhancement.

V. CONCLUSION

In the current paper, the vector magnetic characteristics of ESSs are modeled by means of neural network, and the following work is performed.

1. Through the introduction of the uniform design of experiment method for the determination of the measurement case, the measurement cost and training burden could be lowered considerably.

2. For overcoming the flaws of the convergence accuracy of the algorithm, the conventional back-propagation algorithm is enhanced.

3. For lowering the enhanced BPNN training time further, the original neural network output is split, together with adopting the parallel strategy.

As the verification results indicate, the modeling methodology put forward in the current paper could effectively simulate the vector magnetic characteristics of ESS, and the model possesses good applicability as well. While taking into account the other factors such as frequency, stress and so on, the proposed model is capable of simulating the hysteretic characteristics better and simpler in comparison with the other hysteresis models.

REFERENCES

[1] M. Enokizono, "Vector magneto-hysteresis E&S model and magnetic characteristic analysis," *IEEE Trans. Magn.*, vol. 42, no. 4, pp. 915–918, Apr. 2006, doi: 10.1109/tmag.2006.871667.

[2] W. Li, I. H. Kim, S. M. Jang, and C. S. Koh, "Hysteresis modeling for electrical steel sheets using improved vector Jiles–Atherton hysteresis model," *IEEE Trans. Magn.*, vol. 47, no. 10, pp. 3821–3824, Oct. 2011, doi: 10.1109/TMAG.2011.2158296.

[3] P. Handgruber, A. Stermecki, and O. Bíró, "Anisotropic generalization of vector preisach hysteresis models for non-oriented steels," *IEEE Trans. Magn.*, vol. 51, no. 3, Art. no. 7300604, Mar. 2015, doi: 10.1109/TMAG.2014.2353691.

[4] P. Handgruber, A. Stermecki, O. Biro, V. Gorican, E. Dlala, and G. Ofner, "Anisotropic generalization of vector preisach hysteresis models for nonoriented steels," *IEEE Trans. Magn.*, vol. 51, no. 3, pp. 1–4, Mar. 2015, doi: 10.1109/TMAG.2014.2353691.

[5] M. Kuczmann, "Measurement and simulation of vector hysteresis characteristics," *IEEE Trans. Magn.*, vol. 45, no. 11, pp. 5188–5191, Nov. 2009, doi: 10.1109/tmag.2009.2031072.

[6] L. Zhu, W. Wu, X. Xu, Y. Guo, W. Li, K. Lu, and C.-S. Koh, "An improved anisotropic vector preisach hysteresis model taking account of rotating magnetic fields," *IEEE Trans. Magn.*, vol. 55, no. 6, pp. 1–4, Jun. 2019, doi: 10.1109/TMAG.2019.2899592.

[7] T. Matsuo, "Anisotropic vector hysteresis model using an isotropic vector play model," *IEEE Trans. Magn.*, vol. 46, no. 8, pp. 3041–3044, Aug. 2010, doi: 10.1109/tmag.2010.2043822.

[8] T. Matsuo and M. Miyamoto, "Dynamic and anisotropic vector hysteresis model based on isotropic vector play model for nonoriented silicon steel sheet," *IEEE Trans. Magn.*, vol. 48, no. 2, pp. 215–218, Feb. 2012, doi: 10.1109/tmag.2011.2173751.

[9] L. Zhu, J. Park, and C.-S. Koh, "A dynamic hysteresis model based on vector-play model for iron loss calculation taking the rotating magnetic fields into account," *IEEE Trans. Magn.*, vol. 54, no. 3, pp. 1–4, Mar. 2018, doi: 10.1109/TMAG.2017.2748961.

[10] N. Soda and M. Enokizono, "Improvement of T-joint part constructions in three-phase transformer cores by using direct loss analysis with E&S model," *IEEE Trans. Magn.*, vol. 36, no. 4, pp. 1285–1288, Jul. 2000, doi: 10.1109/20.877675.

[11] M. Enokizono, "Vector magnetic property and magnetic characteristic analysis by vector magneto-hysteretic E&S model," *IEEE Trans. Magn.*, vol. 45, no. 3, pp. 1148–1153, Mar. 2009, doi: 10.1109/tmag.2009.2012659.

[12] Y. Zhang, Y. H. Eum, D. Xie, and C. S. Koh, "An improved engineering model of vector magnetic properties of grain-oriented electrical steels," *IEEE Trans. Magn.*, vol. 44, no. 11, pp. 3181–3184, Nov. 2008, doi: 10.1109/tmag.2008.2001789.

[13] A. Salvini and C. Coltelli, "Prediction of dynamic hysteresis under highly distorted exciting fields by neural networks and actual frequency transplantation," *IEEE Trans. Magn.*, vol. 37, no. 5, pp. 3315–3319, Sep. 2001, doi: 10.1109/20.952603.

[14] A. Salvini and F. R. Fulginei, "Genetic algorithms and neural networks generalizing the Jiles–Atherton model of static hysteresis for dynamic loops," *IEEE Trans. Magn.*, vol. 38, no. 2, pp. 873–876, Mar. 2002, doi: 10.1109/20.996225.

[15] P. Del Vecchio and A. Salvini, "Neural network and Fourier descriptor macromodeling dynamic hysteresis," *IEEE Trans. Magn.*, vol. 36, no. 4, pp. 1246–1249, Jul. 2000, doi: 10.1109/20.877666.

[16] H. H. Saliah, D. A. Lowther, and B. Forghani, "A neural network model of magnetic hysteresis for computational magnetics," *IEEE Trans. Magn.*, vol. 33, no. 5, pp. 4146–4148, Sep. 1997, doi: 10.1109/20.619691.

[17] D. Grimaldi, L. Michaeli, and A. Palumbo, "Automatic and accurate evaluation of the parameters of a magnetic hysteresis model," *IEEE Trans. Instrum. Meas.*, vol. 49, no. 1, pp. 154–160, Feb. 2000, doi: 10.1109/19.836327.

[18] F. Riganti Fulginei and A. Salvini, "Neural network approach for modelling hysteretic magnetic materials under distorted excitations," *IEEE Trans. Magn.*, vol. 48, no. 2, pp. 307–310, Feb. 2012, doi: 10.1109/tmag.2011.2176106.

[19] M. Kuczmann and A. Ivanyi, "A new neural-network-based scalar hysteresis model," *IEEE Trans. Magn.*, vol. 38, no. 2, pp. 857–860, Mar. 2002, doi: 10.1109/20.996221.

[20] W. Laosiritaworn and Y. Laosiritaworn, "Artificial neural network modeling of mean-field ising hysteresis," *IEEE Trans. Magn.*, vol. 45, no. 6, pp. 2644–2647, Jun. 2009, doi: 10.1109/TMAG.2009.2018940.

[21] E. Cardelli, A. Faba, A. Laudani, F. Riganti Fulginei, and A. Salvini, "A neural approach for the numerical modeling of two-dimensional magnetic hysteresis," *J. Appl. Phys.*, vol. 117, no. 17, May 2015, Art. no. 17D129, doi: 10.1063/1.4916306.

[22] E. Cardelli, A. Faba, A. Laudani, G. M. Lozito, F. Riganti Fulginei, and A. Salvini, "Two-dimensional magnetic modeling of ferromagnetic materials by using a neural networks based hybrid approach," *Phys. B, Condens. Matter*, vol. 486, pp. 106–110, Apr. 2016, doi: 10.1016/j.physb.2015.12.005.

[23] Y. Z. Liang, K. T. Fang, and Q. S. Xu, "Uniform design and its applications in chemistry and chemical engineering," *Chemom. Intell. Lab. Syst.*, vol. 58, pp. 43–57, Sep. 2001, doi: 10.1016/s0169-7439(01)00139-3.

[24] R. Li, D. K. J. Lin, and Y. Chen, "Uniform design: Design, analysis and applications," *Int. J. Mater. Product Technol.*, vol. 20, nos. 1–3, pp. 101–114, 2004, doi: 10.1504/ijmpt.2004.003915.

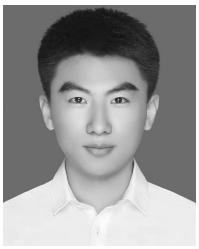

LIANQIANG CHI received the B.S. degree from the University of Science and Technology Liaoning, China, in 2017. He is currently pursuing the M.S. degree with the Shenyang University of Technology. His research interests include magnetic properties measurement and modeling of magnetic material.

DIANHAI ZHANG received the B.S. and M.S. degrees from the Shenyang University of Technology, in 2006 and 2009, respectively, and the Ph.D. degree from Chungbuk National University, in 2013. He is currently an Associate Professor with the Shenyang University of Technology. His research interests include design of electromagnetic devices, and magnetic properties measurement and modeling of magnetic material.

MENGFAN JIA received the M.S. degree from the Shenyang University of Technology, China, in 2019. He is currently an Engineer at the Hunan Provincial Engineering Research Center for electric vehicle motors, CRRC Zhuzhou Electric Company, Ltd. His research interest includes electromagnetic design of PMSM.

ZIYAN REN received the B.S. and M.S. degrees from the Shenyang University of Technology, China, in 2006 and 2009, respectively, and the Ph.D. degree from Chungbuk National University, in 2013. She is currently an Associate Professor with the Shenyang University of Technology. Her research interests include optimal design of electro-magnetic devices and numerical analysis of electromagnetic fields.